1-1-2012

Structural insights into the dehydroascorbate reductase activity of human omega-class glutathione transferases

Huina Zhou
Australian National University

Joseph Brock
Australian National University

Dan Liu
Australian National University

Philip G. Board
Australian National University

Aaron J. Oakley
University of Wollongong, aarono@uow.edu.au

Structural insights into the dehydroascorbate reductase activity of human omega-class glutathione transferases

Abstract

The reduction of dehydroascorbate (DHA) to ascorbic acid (AA) is a vital cellular function. The omega-class glutathione transferases (GSTs) catalyze several reductive reactions in cellular biochemistry, including DHA reduction. In humans, two isozymes (GSTO1-1 and GSTO2-2) with significant DHA reductase (DHAR) activity are found, sharing 64% sequence identity. While the activity of GSTO2-2 is higher, it is significantly more unstable in vitro. We report the first crystal structures of human GSTO2-2, stabilized through site-directed mutagenesis and determined at 1.9Å resolution in the presence and absence of glutathione (GSH). The structure of a human GSTO1-1 has been determined at 1.7Å resolution in complex with the reaction product AA, which unexpectedly binds in the G-site, where the glutamyl moiety of GSH binds. The structure suggests a similar mode of ascorbate binding in GSTO2-2. This is the first time that a non-GSH-based reaction product has been observed in the G-site of any GST. AA stacks against a conserved aromatic residue, F34 (equivalent to Y34 in GSTO2-2). Mutation of Y34 to alanine in GSTO2-2 eliminates DHAR activity. From these structures and other biochemical data, we propose a mechanism of substrate binding and catalysis of DHAR activity.

Keywords

omega, class, activity, reductase, dehydroascorbate, glutathione, into, transferases, insights, structural, human, CMMB

Disciplines

Life Sciences | Physical Sciences and Mathematics | Social and Behavioral Sciences

Publication Details

Zhou, H., Brock, J., Liu, D., Board, P. G. & Oakley, A. J. (2012). Structural insights into the dehydroascorbate reductase activity of human omega-class glutathione transferases. Journal of Molecular Biology, 420 (3), 190-203.

Structural Insights into the Dehydroascorbate Reductase Activity of Human Omega-Class Glutathione Transferases

Huina Zhou[a], Joseph Brock[b], Dan Liu[a], Philip G. Board[a], Aaron J. Oakley[b,c*]

[a]John Curtin School of Medical Research, and [b]Research School of Chemistry, Australian National University, Canberra, ACT 0200, Australia. [c]School of Chemistry, University of Wollongong, Wollongong, NSW 2522, Australia.

Author E-mail addresses: Huina Zhou, joan_zhn@yahoo.com.cn; Joseph Brock, joeylives2ride@gmail.com; Dan Liu, dan.liu@anu.edu.au; Philip G. Board, Philip.Board@anu.edu.au; Aaron J. Oakley, aarono@uow.edu.au.

*Corresponding Author

School of Chemistry, University of Wollongong, Wollongong, NSW 2522, Australia

Telephone: (+61) 2 4221 4347

Fax: (+61) 2 4221 4287

E-mail: aarono@uow.edu.au

Abstract

The reduction of dehydroascorbate (DHA) to ascorbic acid is a vital cellular function. The omega class glutathione transferases catalyze several reductive reactions in cellular biochemistry, including DHA reduction. In humans, two isozymes (GSTO1-1 and GSTO2-2) with significant dehydroascorbate reductase activity are found, sharing 64% sequence identity. While the activity of GSTO2-2 is higher, it is significantly more unstable *in vitro*. We report the first crystal structures of human GSTO2-2, stabilized through site-directed mutagenesis, determined at 1.9 Å resolution in the presence and absence of glutathione. The structure of a human GSTO1-1 has been determined at 1.7 Å resolution in complex with the reaction product ascorbic acid, which unexpectedly binds in the G-site, where the glutamyl moiety of glutathione binds. The structure suggests a similar mode of ascorbate binding in GSTO2-2. This is the first time a non-glutathione-based reaction product has been observed in the G-site of any GST. Ascorbic acid stacks against a conserved aromatic residue, F34 (equivalent to Y34 in GSTO2-2). Mutation of Y34 to alanine in GSTO2-2 eleminates dehydroascorbate reductase activity. From these structures and other biochemical data, we propose a mechanism of substrate binding and catalysis of dehydroascorbate reductase activity.

Keywords: structure; ascorbic acid; reduction; enzyme mechanism; induced fit.

Abbreviations: GST, glutathione transferase; GSH, glutathione; AA, ascorbic acid; DHA, dehydroascorbate; DHAR, dehydroascorbate reductase; COPD, chronic obstructive pulmonary disease.

Introduction

Glutathione transferases (GSTs; E.C. 2.5.1.18) are a major class of phase II detoxification enzymes [1]. Their main function is in the conjugation of endogenous or exogenous xenobiotic toxins with electrophilic centers to glutathione (γ-Glu-Cys-Gly, GSH), but several function as glutathione peroxidases or as reductases [2]. The family of cytosolic GSTs comprises different classes including the omega class [3]. Omega GST is a class with two different subunits (O1 and O2) [4; 5]. The Omega class GSTs have been associated directly with several biological processes including the activation of IL-1β [6] and the modulation of ryanodine receptors [7]. Although the mechanism has not been elucidated, polymorphisms in the Omega class GSTs have been strongly associated with the age at onset of Alzheimer's and Parkinson's diseases [8] and a number of studies have reported associations with a range of disorders including familial amyotrophic lateral sclerosis [9] and the development of acute childhood lymphoblastic leukemia [10]. Specifically, genetic variation in *GSTO2* has been associated with an increased risk of chronic obstructive pulmonary disease (COPD) [11; 12], urothelial carcinoma [13] and in ovarian cancer [14].

GSTO1-1 and GSTO2-2 show novel thiol transferase activity as well as dehydroascorbate (DHA) reductase and monomethylarsenate reductase activities [4; 15; 16; 17]. We have previously shown that GSTO2-2 has higher DHA reductase (DHAR) activity than GSTO1-1 [17] and is considered to be the most active DHAR in mammalian cells. This may be critical in the maintenance of ascorbic acid (AA) levels in the brain since they are dependent on the uptake and subsequent enzymatic reduction of DHA. AA plays a major role in scavenging free radical and specific reactive oxygen species [18] and the high

consumption of oxygen in the brain suggests that a significant capacity to scavenge and detoxify these reactive species is required to prevent oxidative damage. Since the onset of neurological disorders such as Alzheimer's and Parkinson's diseases could be modulated by oxidative stress in the brain it is important to understand the structure and function of enzymes that play a significant role in regulating redox balance. Given the high level of conservation between human GSTO1-1 and GSTO2-2 sequences (64% identity at the amino acid level), it is likely that they operate by the same mechanism. We have previously determined the crystal structure of GSTO1-1 [4] (PDB: 1EEM). Previous attempts to express recombinant human GSTO2-2 met with limited success due to poor expression and instability of the protein [5]. Here, we describe a mutagenesis strategy that was used to improve the solubility and stability properties of GSTO2-2. Non-catalytic cysteine residues predicted to lie on the surface of GSTO2-2 (with potential to destabilize the protein through non-native disulfide bonds) were mutated to serine, and residues at the C-terminus were deleted in order to stabilize the enzyme. The modified protein retains 70% of the wild-type DHAR activity and it was sufficiently stable to enable structural and functional characterization. In order to understand the DHAR activity of omega-class GSTs, we determined the structure of a GSTO1-1 mutant in complex with the reaction product, AA. Together, the data lead us to propose a catalytic mechanism for DHAR activity in omega class GSTs and related enzymes.

Results

Expression, stability and catalytic analysis of GSTO2-2.

Recombinant GSTO2-2 proteins were prepared including wild type GSTO2 (wtGSTO2), GSTO2/MC6 (containing six cysteine to serine mutations), GSTO2/MC6D1 (same as MC6 with the C-terminal cysteine residue deleted), GSTO2/MC6D4 (same as MC6 with four residues as the C-terminus, FGLC, deleted), and GSTO2/D4 (four residues as the C-terminus deleted). The exact modifications present in each mutant are detailed in Table 1. The proteins had varying degrees of solubility. GSTO2/MC6 remained in solution for one day at 4 °C and was comparable with wtGSTO2-2 in the same buffer but did not require 0.5 M arginine as a stabilizing agent. Deletion of C-terminal residues of GSTO2/MC6 in GSTO2/MC6D1 and GSTO2/MC6D4 eliminated the precipitation at high protein concentration (above 5 mg/ml). GSTO2/MC6D1 and GSTO2/MC6D4 gradually precipitated and lost some DHAR activity after four days at 4° C. Protein stability was therefore increased with these modifications, with the most stable protein being GSTO2/MC6D4.

The DHAR activity and the K_M and k_{cat} of wtGSTO2, GSTO2/MC6D1, GSTO2/MC6D4, and GSTO2/D4 were measured to determine if the modifications had a significant impact on function (Table 2). No activity loss was detected for GSTO2/MC6D1 compared with wtGSTO2, while GSTO2/MC6D4 maintained about 70% of wild type DHAR activity. Kinetic studies were limited by the high background rates that occur at high substrate concentrations (see methods) but relative comparisons can be made. MC6D1 and MC6D4 had higher K_{cat}/GSH and K_{cat}/DHA than wtGSTO2-2 and GSTO2/D4 respectively indicating that the six Cys to Ser mutations increase the reaction turnover rate. The Cys to Ser mutations also increased the K_M/GSH but not K_M/DHA, (i.e. DHA binding is

unaffected but the affinity for GSH is reduced). Comparison of GSTO2/D4 and wtGSTO2, as well as GSTO2/MC6D4 and GSTO2/MC6D1, shows that a slightly lower K_M/GSH and a significant lower (50 %) k_{cat} were associated with the deletion of the 4 C-terminal residues. Therefore, modification of the 6 cysteine residues may increase the activity and k_{cat} by stabilizing the protein, while the integrity of the C-terminus may be important for the efficient turnover of the enzyme.

Structure of GSTO2-2

Three structures of GSTO2 have been determined from two crystal forms, in the absence (GSTO2/APO) and presence of GSH bound with partial (GSTO2/GSH) and full (GSTO2/GSH-2) occupancy (Table 3). The GSTO2-2 structures are homodimers (Figure 1a, b) that share common features associated with cytosolic GSTs: an N-terminal thioredoxin-like domain and a C-terminal domain peculiar to the cytosolic GST superfamily (Figure 1c). Structure GSTO2/APO and structure GSTO2/GSH-2 protomers superimpose with a RMSD of 0.52 Å over 236 Cα atoms, demonstrating little perturbation due to different crystal contacts. GSTs typically feature a helix (α2) contributing residues to the G-site. In the GSTO2-structure this is replaced with helix $3_{10}1$, which does not directly interact with GSH (Figure 1c). Like GSTO1, GSTO2 has an extended loop at the N-terminus and two helices at the C-terminus (α8 and $3_{10}3$) that are peculiar to the omega-class enzymes (Figure 1c). The binding location and orientation of GSH in the active sites of GSTO2 is typical of the superfamily (Figure 2b, c). Comparison of the apo- and GSH-bound forms of GSTO2-2 reveal that five water molecules in the G-site are directly displaced by GSH binding. The GSH-cystienyl

amino- and carbonyl-moieties make hydrogen bonds with L72 backbone (Figure 2b, c), and residue L72 is linked to P73 *via* a *cis*-peptide bond (Figure 2a, b, c). These features are observed in all GST structures determined to date. The GSH-glycinyl carboxylate moiety interacts *via* a salt-bridge with K59, located prior to helix $3_{10}1$ in sequence. Several residues contact the GSH γ-glutamyl moiety. The R37 guanadinium-group forms a salt bridge with the GSH γ-glutamyl carboxylic acid group, which also accepts a H-bond from S86 side chain-hydroxyl and main chain-amino groups. The aromatic portion of Y34 interacts with the aliphatic portion of the GSH γ-glutamyl moiety. An unanticipated *cis*-peptide link is observed between residues Y84 and E85 in structures GSTO2/APO and GSTO2/GSH (Figure 2a, b), but not in structure GSTO2/GSH-2 or in GSTO1 (Figure 2c, d), where the usual *trans*-conformation is observed. Residue E85 lies at the C-terminal end of strand β4 in the G-site. The introduction of a *cis*-peptide in structures GSTO2/APO and GSTO2/GSH prevent the E85 amino group from forming a hydrogen bond with the main chain carbonyl oxygen of P73, breaking the β-strand conformation of this residue and causing strand β4 to terminate one residue early (Figure 2a, b). In the GSTO2/APO and GSTO2/GSH structures, the E85 carboxylate interacts with the H71 imidazole ring (Figure 2a, b). In structure GSTO2/GSH-2, it is partially disordered, and two conformations are observed. Both conformers form a salt-bridge with the γ-glutamyl amino group of GSH (Figure 2c). The omega-class GSTs possess an active site cysteine (C32 in GSTO2) that forms a mixed disulfide with GSH, which is observed in structures GSTO2/GSH and GSTO2/GSH-2, and in GSTO1-1 (Figure 2b, c, d). C32 is located at the N-terminus of helix α1, with its thiol-group positioned over the helix axis.

The H-site in GSTO2-2 (Figure 2a, b, c) is co-localized with the equivalent site in GSTO1-1 (Figure 2d) and other GST classes. The N-terminal domain contributes residues F31 and P33 to the site. Residues R184 and Y188, at the C-terminal end of helix α6, form one wall of the cavity. A well-ordered water molecule found in the cavity in all 3 structures accepts hydrogen bonds from the R184-Nε and Y188-Oη groups, and donates a hydrogen bond to the F31 carbonyl (Figure 2a, b, c). The H-site is completed by residues from helix α8: F223, F226, L227 and Y230. In structure GSTO2/GSH-2, density lying between P33, F226 and Y230 was modeled as ethylene glycol. Comparison of structures GSTO2/APO and GSTO2/GSH show that 11 residues up to the C-terminus (which includes the C-terminal 4 residues of helix α8) become disordered upon GSH binding (Fig. 2b), however, no such disorder is observed in structure GSTO2/GSH-2. The reasons for this are not clear, but may involve different crystal contacts between GSTO2/APO and GSTO2/GSH ($P2_1$ symmetry) and GSTO2/GSH-2 ($P6_522$ symmetry). In structure GSTO2/APO, the C-terminal end of helix α8 forms crystal contacts. In structure GSTO2/GSH-2, helix $3_{10}3$ and parts of helix α8 are stabilized through crystal contacts.

Crystal structure of GSTO1-1 with ascorbic acid

The structure of GSTO1-1 C32S mutant with AA has been determined at 1.70 Å resolution (Table 3). In this structure, AA engages in π-stacking with F34, 5 Å from the mutated C32S residue, occupying a portion of the 'G-site' that typically binds the γ-glutamyl moiety of GSH (Figure 2d). The opposite face of AA contacts the side chain of L71 (Figure 2e). The only significant structural perturbation with reference to the

GSTO1/GSH structure [4] is the altered conformer of E85, which is observed in two conformers, one the same as in the GSH-bound form of the enzyme and the second in a new conformation engaged in hydrogen-bonding interactions with the C6-hydroxyl of ascorbate and the side-chain hydroxyl of S86. The main chain amide of S86 also forms a hydrogen bond with its C5-hydroxyl. Other interactions within the active site include a hydrogen bond between its C3-hydroxyl group and the backbone carbonyl of V72. Electron density adjacent to AA was interpreted as an acetate ion, present in the buffer. One oxygen atom of the acetate ion was 2.65 Å from the serine hydroxyl group, and mediates an interaction between the S32-hydroxyl group and the C2-hydroxyl of ascorbate (Figure 2e). The other oxygen atom forms a hydrogen bond with a water molecule in the H-site. The methyl group of the acetate group stacks against the side of F34-phenyl group.

Comparisons of GSTO2 with GSTO1

The GSTO2 structure is broadly similar to that of GSTO1. Protomers of GSTO1 and GSTO2 structure GSTO2/GSH superimpose with a RMSD of 0.934 Å over 227 Cα atoms. Several features first observed in GSTO1 are conserved in GSTO2. These include the N-terminal extension that stacks against the side of the β-sheet and the α8- and 3_{10}3-helices that contributes to the distinctive shape of the active site (Figure 1c). The dimer interface of GSTO2-2 is slightly wider than that of GSTO1-1. Helix α4, the first helix in the C-terminal domain is kinked in both GSTO1 and 2. The G-sites of both isozymes are similar. The most significant differences between GSTO1 and O2 are found in the H-sites of the two enzymes. Relative to GSTO1, helix α8 in GSTO2 is shifted away from the G-site by about 1.5 Å (Figure 2c, d). Residue Y230 in GSTO2 is rotated up and away from

the G-site compared with the equivalent Y229 in GSTO1. F223 in GSTO2 is substituted with W222 in GSTO1. The substitution of Y188 in GSTO2 with M187 in GSTO1 (Figure 2d) creates space for the bulkier W222 side chain. These substitutions result in altered patterns of hydrogen bond donors in the two enzymes. GSTO2 has lost a hydrogen-bond donor due to the substitution of W222 for F223, and gained a hydrogen bond donor Y188-Oη. This donor, together with the hydrogen bond acceptor F31O and donor R184-Nε create the novel pocket that stabilizes a water molecule found in all GSTO2 structures. One point of similarity in the H-sites of the two isozymes is the W180 residue and a structurally conserved water molecule that accepts a hydrogen bond from the side-chain amino group of this residue (Figure 2c, d). Both GSTO1-1 and GSTO2-2 have positive electrostatic potential in their H-sites, although some differences were observed (Figure 3). This can be explained by substitution of R132 in GSTO1 with valine in GSTO2. Conversely, GSTO2 has gained a positive charge through substitution in the form of a lysine residue at position 128 (equivalent to G128 in GSTO1). The active site of GSTO2-2 is more occluded compared with GSTO1-1 due to the latter substitution and the rotation of residue Y230 (Y229 in GSTO1) into the opening of the H-site (Figure 2c). This rotation is caused by the substitution of C237 (in the C-terminal 3_{10}-helix of GSTO1) with a phenylalanine residue in GSTO2.

Mutation of GSTO2 G-site residues

To probe the significance of residues E85 and Y34 in GSTO2-2, two point mutants were created based on the GSTO2/MC6D1 construct: GSTO2/MC6D1-E85A and GSTO2/MC6D1-Y34A. The E85A mutation of the GSTO2/MC6D1 protein diminished

the DHAR activity by about 50 %. DHAR activity is eliminated in the Y34A mutant. Circular dichroism (data not shown) confirmed that the lack of activity was not due to misfolding.

Discussion

The importance of human omega-class GSTs in reductive biochemistry, and their involvement in Alzheimer's and other diseases make them a worthy target for structural and functional characterization. The structure of hGSTO1 was reported previously [4], and here, we present the structure of hGSTO2-2 stabilized by mutagenesis. Although GSTO1 and GSTO2 share over 60% sequence identity, they have different substrate specificities [5; 19]. It appears likely that the differences in activity of the two isozymes are likely due to the differences in the H-sites described above. The location of Y230 and K128 in GSTO2 creates a narrower entrance to the H-site, (Figure 2c, d). This reduction is consistent with the observed preference of GSTO2 for smaller substrates in comparison to GSTO1 [5; 19]. The conservation of an H-site water molecule in GSTO1 and O2, hydrogen bonded to W180-Nε1 may suggest a functionally conserved role (Figure 2c,d).

Comparison of crystals structures of GSTO2-2 with unoccupied-, partially- and fully-occupied G-sites allow changes due to GSH binding to be observed. No significant perturbations were observed upon GSH binding, with the exception of E85, which is in a *cis*-conformation in structures GSTO2/APO and GSTO2/GSH and in the *trans*-conformation in GSTO2/GSH-2 (Figure 2a, b, c). In the latter case, the side-chain of E85 forms a salt-bridge with the amino-group of the GSH-γ-glutamyl amino-moiety. These

observations hint at a novel induced-fit mechanism in GSTO2. Alternately, these structures may represent snapshots of the dynamic changes that occur in the protein in solution, the different forms of which are selected in the crystallization process. While the side chain of E85 contributes to the DHA reductase activity of the protein, the activity of the E85A mutant indicates that it is non-essential. The ability of the Y84-E85 peptide bond to adopt a *cis*-conformation could be responsible for the higher DHAR activity of GSTO2-2 compared with GSTO1-1. If the *cis*-conformation is favored in solution for GSTO2-2, E85 may be ideally pre-positioned to bind DHA, whereas in GSTO1-1, the side-chain must change conformation to interact with AA (Figure 2d, e).

The observation of disorder in the C-terminal region structure GSTO2/GSH warrants comment. While crystal-packing effects cannot be ruled out, this phenomenon may reflect the inherent flexibility of this region of the protein. Instability in the C-terminal region of the wild-type protein, containing the four C-terminal residues FGLC, could lead to aggregation through non-specific hydrophobic interactions.

Modified hGSTO2-2 (GSTO2/MC6D4) retains ~70% of the DHAR activity of wild type enzyme. Even though none of the modifications are found in the G- or H-site, they do have some effects on DHAR activity of GSTO2. The Cys to Ser mutations decrease the GSH affinity of the G-site but increase enzyme turnover rate, with a net higher reductase activity. Deletion of C-terminal FGLC residues reduces the enzyme turnover rate to less than half of the wild-type enzymes and increased the GSH affinity. While there is no indication that these residues could directly interact with GSH, the truncation could act to

destabilize the C-terminal region (as was observed in the GSTO2/GSH structure), leading to indirect effects on GSH binding. An induced-fit mechanism of GSH with the C-terminus of the human GSTA1-1 has been observed [20]. Notably, modifications to GSTO2 made here have little effect on DHA-binding.

Given their importance in reductive biochemistry, we sought to understand the DHAR activity of omega-class GSTs. The nature of DHA itself makes analysis of enzyme-substrate interactions difficult: DHA reacts with water to form homicidal species (Figure 4a) [21]. Furthermore, DHA is unstable, degrading to several products *via* diketogulonic acid [22]. A further complication arises from the formation of GSH-conjugates from these intermediates [23]. We therefore pursued the structure of an omega-class GST with the more stable reaction product, AA. The binding of AA in the G-site of GSTO1-1 was unanticipated. Its occlusion of the G-site suggests product inhibition, an observation that contrasts with studies on the homologous *Arabidopsis* DHAR, where no evidence was found of product inhibition by Dixon and co-workers [24]. However, the concentration of AA used here was much higher: 100 mM *versus* 5 mM by Dixon and co-workers. The binding of AA suggests that the enolic tautomeric form of DHA (protonated at O3) binds in the G-site as observed for AA (Figure 4b). An OH group at the 3'-position is able to donate a hydrogen bond to the P73 carbonyl oxygen. A mechanism of *Arabidopsis* DHAR activity involving this tautomer of DHA has been outlined by Dixon and coworkers [24], and an analogous mechanism may operate in the omega-class GSTs in which the anionic form of C32 donates an electron to DHA to give the stable semidehydroascorbate radical, a well known intermediate in AA oxidation [22] (Figure 4c).

Abstraction of hydrogen from GSH results in AA formation. The resulting thiyl radicals of GS˙ and C32-S˙ would then terminate to form the glutathione-enzyme mixed disulfide. An alternative concerted mechanism is shown in Figure 4c. DHA is displaced by GSH binding with the concomitant reduction of DHA to AA by the enzyme and GSH, and a mixed enzyme/GSH disulfide is formed.

In our model of DHA binding, the π-stacking interaction of DHA with F34 plays a crucial role: the π-stacking interaction would promote dehydration of the hemiacetal forms that would not interact favorably with the aromatic ring. In our model of DHA binding, GSH sulfhydryl must approach the exposed *si* face, giving the correct stereocenter at C4 upon transfer of hydrogen. Further evidence for the role of this aromatic group comes from the inactivity of the Y34A mutant. The mechanism is consistent with kinetic analysis of the spinach chloroplast DHAR (a GSTO homolog) which suggests binding of DHA to the reduced form of the enzyme prior to GSH [25]. The activity of spinach chloroplast DHAR was inhibited by incubation with iodoacetic acid, shown to modify C23 (equivalent to C32 in GSTO1 and 2). This modification was suppressed by the addition of DHA, suggesting binding of this substrate close to this residue [25] which is consistent with our observation of AA binding close to C32 in GSTO1. The use of only the G-site for binding of both substrates is consistent with the lack of H-sites in proteins such as glutaredoxins, which contain G-site but not an H-site. The recently reported *Phanerochaete chrysosporium* GSTO1 structure has an H-site that appears largely occluded by the side-chains of tyrosine residues [26]. This enzyme catalyzes DHA reduction and has a tryptophan residue (W88) in place of tyrosine (Y34) or

phenylalanine (F34) in GSTO2 and O1 respectively. The mechanism is consistent with conserved features in GSTO and all homologues with DHAR activity, including G-site *cis*-proline, G-site aromatic residue (F34 in GSTO1), and essential reactive cysteine (Figure 5). Our proposed mechanism does not involve a thiohemiketal intermediate, which was proposed for porcine glutaredoxin (thioltransferase) [27], since formation of a thiohemiketal would likely result in a dead-end thioketal-enzyme complex [24].

Materials and Methods

Wild type protein expression and purification for GSTO2-2

Human GSTO2 with a 6xHis tag was expressed in *E. coli* M15/rep4 cells using plasmid pQE30 (Qiagen) under control of the T5 promoter [5]. Cultures were grown at 16 °C. The protein was purified as described previously [4] with some modifications. Briefly, cells were harvested by centrifugation (4000 g for 10 min at 4 °C) and resuspended in lysis buffer (phosphate buffered saline containing 15% glycerol, 0.3 M NaCl, 20 mM imidazole). Cells were lysed by passage through a French pressure cell and insoluble material was removed by centrifugation. All purification steps were undertaken at 4° C. The clarified lysate was mixed with Ni-NTA sepharose (50% slurry) equilibrated in the lysis buffer for 1 hour on a rotary mixer. Unbound protein was removed from the Ni-NTA sepharose by copious washing on a sintered glass funnel. The washed sepharose beads were then placed in a chromatography column and the recombinant GSTO2-2 was eluted using lysis buffer containing 0.25 M imidazole, pH 7. Upon elution, arginine was

added to a final concentration of 0.5 M to prevent precipitation and encourage refolding. The purified protein was concentrated on a Falcon concentrator (BD Biosciences) to at least 10 mg/ml. The purity of the purified protein was assessed by SDS-PAGE and the protein was stored at -70° C. No activity loss was detected after 2 years of storage. In the absence of arginine and glycerol the protein precipitated quickly.

Site-directed mutagenesis, purification and crystallization of GSTO2-2

The consistent precipitation of the wild type GSTO2-2 protein during crystallization trials led us to investigate possible causes and remedies. Human GSTO2 has 11 cysteine residues compared with 5 in GSTO1. Beginning with the hypothesis that the abundance of cysteine residues contributed to the protein's instability, a model of GSTO2 was made using GSTO1 as a template in order to identify cysteine residues not near the active site and likely to be exposed to solvent. These were selected for mutation to serine. The following residues were mutated: C80, C121, C136, C140, C170, C214, to give "GSTO2/MC6". A second construct "GSTO2/MC6D1" was created which contained the six aforementioned Cys to Ser mutations and deletion of the C-terminal residue (Cys243). Finally, a third construct "GSTO2/MC6D4" was made containing the six Cys to Ser mutations and the deletion of four residues (FGLC) at the C-terminus. To verify the effects of mutations and deletions on protein stability and activity, an extra construct "GSTO2/D4" was made only containing the deletion of four residues at C-terminus. To assess its functional importance, the strictly conserved G-site residue E85 (usually either E or Q in the cytosolic GST family) was mutated to A in the GSTO2/MC6D1 construct to create GSTO2/MC6D1-E85A. Similarly, to assess the importance of Y34 in the DHAR reaction mechanism it was mutated to A to create GSTO2/MC6D1-Y34A. All constructs

were cloned in pQE30 plasmid and expressed in *E. coli* M15/rep4 cells. The purified proteins retain a 6xH tag at the N-terminal. The primers used for these mutations are listed in Table 4.

The modified enzymes were expressed as soluble proteins at 37° C after induction by 0.1 mM isopropyl-β-D-thiogalactopyranoside (IPTG). Proteins were purified as described for wild-type GSTO2-2 with some modifications to the buffer. Initial crystallization screens using wild type GSTO2-2 were unsuccessful. Examination of crystallization drops revealed that 2-Methyl-2,4-pentanediol (MPD) had a solublising effect on the protein. MPD was therefore added to the purification buffer. The modified GSTO2-2 proteins giving best crystals were obtained by Ni-affinity chromatography with the following buffer: 0.3 M NaCl, 25 mM imidazole, 3 % glucose, 5 % glycerol, 5 % MPD, 0.1 M MOPS pH 7.0. The elution buffer was identical except for the addition of imidazole to a concentration of 0.3 M. The purified protein was concentrated by dialysis against PEG 7000-9000 using a 10 kDa cutoff dialysis membrane at 4° C overnight. The purity of proteins was assessed by SDS-PAGE and gel filtration on a Superose-12 column (Pharmacia). Recombinant wild-type GSTO2-2 is very unstable and precipitates during the purification procedure. The improved relative stability of the mutant isoforms was evaluated by their capacity to resist precipitation and inactivation during purification and during storage at 4° C.

Crystallization screens were performed on the GSTO2/MC6D1 and GSTO2/MC6D4 proteins that had been concentrated to around 10 mg/ml. The sitting-drop vapor diffusion

method in a 96 well tray format as used with Crystal Screens 1 and 2 (Hampton Research, CA). Equal volumes (1 μl) of protein and reservoir solution were mixed in the drop receptacles prior to sealing the tray for equilibration at 4° C. For X-ray data collection, crystals were grown by the hanging-drop vapor diffusion method using 24-well trays (Greiner Bio-One, CA) at 18° C. Solutions of protein and precipitant (1.5 μl each) were mixed on siliconized cover slips (Hampton Research) prior to suspension over 0.5 ml of reservoir solution. Microseeds were made by the ultrasonicated bead method [28] and used to assist the discovery of crystallization conditions: screening was performed as described above except with the addition of 0.1 μl of seed solution.

While variants GSTO2/MC6D1 and GSTO2/MC6D4 were subjected to crystallization trials, only GSTO2/MC6D4 gave diffraction-quality crystals. The best crystals were found with condition 46 of Crystal Screen 2 (0.1 M sodium chloride, 0.1 M Bicine pH 9.0, 20 % (w/v) PEGMME 2000). Optimal crystals grown using the hanging-drop vapor diffusion technique were rods of dimension 30 × 30 × 200 μm. One data set (GSTO2/APO) was collected from a single crystal of GSTO2/MC6D4, and a second collected (GSTO2/GSH) from a crystal grown under the same conditions but with 20 mM GSH added (see below). A second crystal habit (hexagonal bipyramids) was found with condition 39 of Crystal Screen 1 (0.1M Hepes pH7.5, 2% v/v Polyethylene glycol 400, 2M ammonium sulfate). These crystals appeared upon microseeding with monoclinic crystals sourced from condition 46 of Crystal Screen 2. Optimal numbers and sizes of crystals were obtained using a 1000-fold dilution of seed stock and a protein concentration of about 5 mg/ml with 20 mM GSH in condition 39 of Crystal Screen 1.

The best crystals had dimension 30 × 30 × 30 μm and a dataset (GSTO2/GSH-2) was collected from one of these crystals as described below.

Site-directed mutagenesis, Purification and crystallization of GSTO1-1

Repeated soaking experiments of wild-type human GSTO1, and GSTO2/MC6D4 crystals failed to yield a crystal structure with bound AA. Hypothesizing that a catalytically incompetent mutant might allow visualization the reaction product, we created a GSTO1-C32S mutant, which is unable to form a mixed-disulfide with GSH. The construct was cloned into the pHUE vector and expressed as a 6xHis-tagged fusion protein with ubiquitin in *E. coli* BL21 cells as described previously [29]. The primers used to make the C32S mutation are shown in Table 4. Protein expression was induced by 50 μM IPTG at 37 °C and purified using Ni-affinity chromatography. Finally the 6x-His-ubiquitin portion was cleaved and removed as described previously [29]. Protein solutions were dialysed overnight against 60 mM NaCl, 20 mM Tris, 5 mM DTT, pH 8 at 4 °C before concentrating to 25 mg/ml using a 10 kDa cutoff Amicon Ultra centrifugal device (Millipore, Cork, Ireland). Purity was assessed by SDS-PAGE.

The hGSTO1-1 C32S mutant was crystallized using the hanging drop vapor diffusion method. Optimal crystal growth was modified from conditions previously published [4]. The reservoir consisted 2.2 M $(NH_4)_2SO_4$ and 100 mM Sodium Acetate, pH 4.75. 1 μl of protein was mixed with 1 μl L-ascorbate (100 mM), 1 μl of a saturated solution of α-tocopherol succinate (an uncompetitive inhibitor [30]) and 1 μl of reservoir solution.

X-ray data Collection and crystal structure determination

All X-ray data were collected at the Australian synchrotron, beam line MX1. Crystal structures of GSTO2 were solved by molecular replacement using PHASER [31]. REFMAC [32] was used for structure refinement including TLS refinement [33]. Occupancy refinement was performed in PHENIX [34]. Model building and electrostatic surface calculations were performed using COOT [35].

Diffraction data of Crystals GSTO2/APO and GSTO2/GSH were processed by MOSFLM of CCP4 suite [36]. Crystals GSTO2/GSH-2 and GSTO1/AA was processed using the HKL package [37]. The structure GSTO2/APO was solved using the hGSTO1 crystal structure (PDB id 1EEM). The crystals belong to space group of $P2_1$ with a physiological dimer in the asymmetric unit. After several rounds of restrained refinement in REFMAC and manual model building in COOT, the R and R_{free} reduced to 0.19 and 0.24 respectively. An ethylene glycol monomer, one glycerol molecule and two chloride ions were added to the model together with water molecules in the final stages of model building. No GSH was observed to bind in the G-site. This structure was used as the starting model for structures GSTO2/GSH and GSTO2/GSH-2. Structure GSTO2/GSH was isomorphous with structure GSTO2/APO. Additional density (>1σ) in the $2mF_o$-DF_c was observed in the active sites in both protomers, corresponding to GSH binding. Good density was observed for the γ-glutamyl and cysteinyl residues, but electron density was poor for the glycine moiety. Occupancy refinement in PHENIX suite gave partial occupancy of 0.62 and 0.71 for GSH in each G-site. Two PEG molecules and chloride ions were added to structure GSTO2/GSH-2 in addition to water molecules. Initial processing of dataset GSTO2/GSH-2 revealed a hexagonal Bravis lattice. Merging in SCALEPACK and examination of systematically absent reflections indicated space group

$P6_122$ or its enantiomorph $P6_522$. The correct space group ($P6_522$) was identified by PHASER. The asymmetric unit contained a GSTO2/MC6D4 protomer, which lies upon a crystallographic 2-fold axis to give a physiological dimer. Inspection of $2mF_o$-DF_c electron density maps revealed clear (>1.5σ) electron density for GSH. The GSTO1/AA structure is isomorphous with the previously reported structure of GSTO1 with GSH [4] (PDB: 1EEM). This structure, with ligands and water molecules removed, was used as the starting model for refinement. Sulfate and glycerol molecules were built into the model and AA was included in the final stages of refinement. All refinement statistics were shown in Table 3.

Enzyme activity assay

Dehydroascorbate reductase (DHAR) activity was measured spectrophotometrically by recording the increase in absorbance at 265 nm as described previously [17]. The reaction mix contained of 200mM Na phosphate and 1mM EDTA, pH6.85, 2.25mM GSH, and 1mM DHA in a total volume of 1 ml. The reaction was started by the addition of DHA and recorded for 2 minutes at 30°C with a 1cm light path. The reaction rate was calculated using an extinction coefficient of 14.7mM/cm. DHA was prepared from ascorbic acid immediately before use as previously described [38].

For the determination of the Michaelis-Menten constant (K_m) for GSH, the DHA concentration was kept to 1mM, while GSH concentration was varied from 0.25 mM to 4 mM. For the K_M of DHA, GSH concentration was kept at 2.25 mM, while DHA was varied from 0.1 to 2 mM. Because very high back round rates occur at high GSH and high DHA concentrations the reaction rates could not be determined under saturating conditions. Consequently the concentration of GSH used for the determination of the K_m

(DHA) was below the K_m (GSH) and not saturating. As a result the K_{cat} was lower when DHA was varied than when GSH was varied and the values are presented separately in Table2. Despite the non-saturating conditions, relative comparisons between the mutated isoforms can still be made

Accession numbers

All structures and X-ray structure factors have been deposited at the PDB. Accession numbers: **3Q18**, **3Q19**, **3QAG** and **3VLN**.

Acknowledgments

X-ray data were collected on the MX1 beamline at the Australian Synchrotron, Victoria, Australia. This work was supported by National Health and Medical Research Council Project Grant 366731.

References

1. Oakley, A. (2011). Glutathione transferases: a structural perspective. *Drug Metab Rev* **43**, 138-51.
2. Oakley, A. J. (2005). Glutathione transferases: new functions. *Current Opinion in Structural Biology* **15**, 716-723.
3. Hayes, J. D., Flanagan, J. U. & Jowsey, I. R. (2005). Glutathione transferases. *Annu Rev Pharmacol Toxicol* **45**, 51-88.
4. Board, P. G., Coggan, M., Chelvanayagam, G., Easteal, S., Jermiin, L. S., Schulte, G. K., Danley, D. E., Hoth, L. R., Griffor, M. C., Kamath, A. V., Rosner, M. H., Chrunyk, B. A., Perregaux, D. E., Gabel, C. A., Geoghegan, K. F. & Pandit, J. (2000). Identification, Characterization and Crystal structure of the Omega Class Glutathione Transferases. *J Biol Chem* **275**, 24798-24806.
5. Whitbread, A. K., Tetlow, N., Eyre, H. J., Sutherland, G. R. & Board, P. G. (2003). Characterization of the human Omega class glutathione transferase genes and associated polymorphisms. *Pharmacogenetics* **13**, 131-44.
6. Laliberte, R. E., Perregaux, D. G., Hoth, L. R., Rosner, P. J., Jordan, C. K., Peese, K. M., Eggler, J. F., Dombroski, M. A., Geoghegan, K. F. & Gabel, C. A. (2003). Glutathione s-transferase omega 1-1 is a target of cytokine release inhibitory drugs and may be responsible for their effect on interleukin-1beta posttranslational processing. *J Biol Chem* **278**, 16567-78.

7. Dulhunty, A., Gage, P., Curtis, S., Chelvanayagam, G. & Board, P. (2001). The Glutathione Transferase Structural Family Includes a Nuclear Chloride Channel and a Ryanodine Receptor Calcium Release Channel Modulator. *J Biol Chem* **276**, 3319-3323.
8. Li, Y. J., Scott, W. K., Hedges, D. J., Zhang, F., Gaskell, P. C., Nance, M. A., Watts, R. L., Hubble, J. P., Koller, W. C., Pahwa, R., Stern, M. B., Hiner, B. C., Jankovic, J., Allen, F. A., Jr., Goetz, C. G., Mastaglia, F., Stajich, J. M., Gibson, R. A., Middleton, L. T., Saunders, A. M., Scott, B. L., Small, G. W., Nicodemus, K. K., Reed, A. D., Schmechel, D. E., Welsh-Bohmer, K. A., Conneally, P. M., Roses, A. D., Gilbert, J. R., Vance, J. M., Haines, J. L. & Pericak-Vance, M. A. (2002). Age at onset in two common neurodegenerative diseases is genetically controlled. *Am J Hum Genet* **70**, 985-93.
9. van de Giessen, E., Fogh, I., Gopinath, S., Smith, B., Hu, X., Powell, J., Andersen, P., Nicholson, G., Al Chalabi, A. & Shaw, C. E. (2008). Association study on glutathione S-transferase omega 1 and 2 and familial ALS. *Amyotroph Lateral Scler* **9**, 81-4.
10. Pongstaporn, W., Pakakasama, S., Sanguansin, S., Hongeng, S. & Petmitr, S. (2009). Polymorphism of glutathione S-transferase Omega gene: association with risk of childhood acute lymphoblastic leukemia. *J Cancer Res Clin Oncol* **135**, 673-8.
11. Wilk, J. B., Walter, R. E., Laramie, J. M., Gottlieb, D. J. & O'Connor, G. T. (2007). Framingham Heart Study genome-wide association: results for pulmonary function measures. *BMC Med Genet* **8 Suppl 1**, S8.
12. Yanbaeva, D. G., Wouters, E. F., Dentener, M. A., Spruit, M. A. & Reynaert, N. L. (2009). Association of glutathione-S-transferase omega haplotypes with susceptibility to chronic obstructive pulmonary disease. *Free Radic Res* **43**, 738-43.
13. Wang, Y. H., Yeh, S. D., Shen, K. H., Shen, C. H., Juang, G. D., Hsu, L. I., Chiou, H. Y. & Chen, C. J. (2009). A significantly joint effect between arsenic and occupational exposures and risk genotypes/diplotypes of CYP2E1, GSTO1 and GSTO2 on risk of urothelial carcinoma. *Toxicol Appl Pharmacol* **241**, 111-8.
14. Pongstaporn, W., Rochanawutanon, M., Wilailak, S., Linasamita, V., Weerakiat, S. & Petmitr, S. (2006). Genetic alterations in chromosome 10q24.3 and glutathione S-transferase omega 2 gene polymorphism in ovarian cancer. *J Exp Clin Cancer Res* **25**, 107-14.
15. Whitbread, A. K., Masoumi, A., Tetlow, N., Schmuck, E., Coggan, M. & Board, P. G. (2005). Characterization of the omega class of glutathione transferases. *Methods Enzymol* **401**, 78-99.
16. Zakharyan, R. A., Sampayo-Reyes, A., Healy, S. M., Tsaprailis, G., Board, P. G., Liebler, D. C. & Aposhian, H. V. (2001). Human monomethylarsonic acid (MMA(V)) reductase is a member of the glutathione-S-transferase superfamily. *Chem Res Toxicol* **14**, 1051-7.
17. Schmuck, E. M., Board, P. G., Whitbread, A. K., Tetlow, N., Cavanaugh, J. A., Blackburn, A. C. & Masoumi, A. (2005). Characterization of the monomethylarsonate reductase and dehydroascorbate reductase activities of Omega class glutathione transferase variants: implications for arsenic metabolism

and the age-at-onset of Alzheimer's and Parkinson's diseases. *Pharmacogenet Genomics* **15**, 493-501.
18. Frei, B., England, L. & Ames, B. N. (1989). Ascorbate is an outstanding antioxidant in human blood plasma. *Proc Natl Acad Sci U S A* **86**, 6377-81.
19. Board, P. G., Coggan, M., Cappello, J., Zhou, H., Oakley, A. J. & Anders, M. W. (2008). S-(4-Nitrophenacyl)glutathione is a specific substrate for glutathione transferase omega 1-1. *Anal Biochem* **374**, 25-30.
20. Cameron, A. D., Sinning, I., L'Hermite, G., Olin, B., Board, P. G., Mannervik, B. & Jones, T. A. (1995). Structural analysis of human alpha-class glutathione transferase A1-1 in the apo-form and in complexes with ethacrynic acid and its glutathione conjugate. *Structure* **3**, 717-27.
21. Doner, L. W. & Hicks, K. B. (1981). High-performance liquid-chromatographic separation of ascorbic-acid, erythorbic acid, dehydroascorbic acid, dehydroerythorbic acid, diketogulonic acid, and diketogluconic acid. *Analytical Biochemistry* **115**, 225-230.
22. Winkler, B. S., Orselli, S. M. & Rex, T. S. (1994). The Redox Couple Between Glutathione and Ascorbic-Acid - A Chemical and Physiological Perspective. *Free Radical Biology and Medicine* **17**, 333-349.
23. Regulus, P., Desilets, J. F., Klarskov, K. & Wagner, J. R. (2010). Characterization and detection in cells of a novel adduct derived from the conjugation of glutathione and dehydroascorbate. *Free Radic Biol Med* **49**, 984-91.
24. Dixon, D. P., Davis, B. G. & Edwards, R. (2002). Functional divergence in the glutathione transferase superfamily in plants. Identification of two classes with putative functions in redox homeostasis in Arabidopsis thaliana. *J Biol Chem* **277**, 30859-69.
25. Shimaoka, T., Miyake, C. & Yokota, A. (2003). Mechanism of the reaction catalyzed by dehydroascorbate reductase from spinach chloroplasts. *Eur J Biochem* **270**, 921-8.
26. Meux, E., Prosper, P., Ngadin, A., Didierjean, C., Morel, M., Dumarcay, S., Lamant, T., Jacquot, J. P., Favier, F. & Gelhaye, E. (2011). Glutathione transferases of Phanerochaete chrysosporium: S-glutathionyl-p-hydroquinone reductase belongs to a new structural class. *J Biol Chem* **286**, 9162-73.
27. Washburn, M. P. & Wells, W. W. (1999). Identification of the dehydroascorbic acid reductase and thioltransferase (Glutaredoxin) activities of bovine erythrocyte glutathione peroxidase. *Biochem Biophys Res Commun* **257**, 567-71.
28. Luft, J. R. & DeTitta, G. T. (1999). A method to produce microseed stock for use in the crystallization of biological macromolecules. *Acta Crystallogr D Biol Crystallogr* **55**, 988-93.
29. Baker, R. T., Catanzariti, A. M., Karunasekara, Y., Soboleva, T. A., Sharwood, R., Whitney, S. & Board, P. G. (2005). Using deubiquitylating enzymes as research tools. *Methods Enzymol* **398**, 540-54.
30. Sampayo-Reyes, A. & Zakharyan, R. A. (2006). Tocopherol esters inhibit human glutathione S-transferase omega. *Acta Biochim Pol* **53**, 547-52.
31. McCoy, A. J., Grosse-Kunstleve, R. W., Adams, P. D., Winn, M. D., Storoni, L. C. & Read, R. J. (2007). Phaser crystallographic software. *J Appl Crystallogr* **40**, 658-674.

32. Murshudov, G. N., Vagin, A. A. & Dodson, E. J. (1997). Refinement of macromolecular structures by the maximum-likelihood method. *Acta Crystallographica Section D-Biological Crystallography* **53**, 240-255.
33. Winn, M. D., Isupov, M. N. & Murshudov, G. N. (2001). Use of TLS parameters to model anisotropic displacements in macromolecular refinement. *Acta Crystallographica Section D-Biological Crystallography* **57**, 122-133.
34. Adams, P. D., Grosse-Kunstleve, R. W., Hung, L. W., Ioerger, T. R., McCoy, A. J., Moriarty, N. W., Read, R. J., Sacchettini, J. C., Sauter, N. K. & Terwilliger, T. C. (2002). PHENIX: building new software for automated crystallographic structure determination. *Acta Crystallogr D Biol Crystallogr* **58**, 1948-54.
35. Emsley, P. & Cowtan, K. (2004). Coot: model-building tools for molecular graphics. *Acta Crystallogr D Biol Crystallogr* **60**, 2126-32.
36. Bailey, S. (1994). The Ccp4 Suite - Programs for Protein Crystallography. *Acta Crystallographica Section D-Biological Crystallography* **50**, 760-763.
37. Otwinowski, Z. & Minor, W. (1997). Processing of X-ray Diffraction Data Collected in Osillation Mode. In *Methods in Enzymology* (Carter, C. W. & Sweet, R. M., eds.), Vol. 276, pp. 307-326. Academic Press, New York.
38. Wells, W. W., Xu, D. P. & Washburn, M. P. (1995). Glutathione: dehydroascorbate oxidoreductases. *Methods Enzymol* **252**, 30-8.
39. Humphrey, W., Dalke, A. & Schulten, K. (1996). VMD: Visual molecular dynamics. *Journal of Molecular Graphics* **14**, 33-38.

Figure Legends

Figure 1. Cartoon representation of the GSTO2/MC6D4. Shown are the dimer (a), with an orthogonal view (b), and protomer with secondary structure labels (c). GSH is shown in stick form. All figures were drawn using VMD [39]. In (c) the N-terminal and C-terminal regions peculiar to the omega-class GSTs are highlighted in green red respectively.

Figure 2. Stereodiagrams of GSTO active sites. The active sites of (a) GSTO2/APO, (b) GSTO2/GSH, (c) GSTO2/GSH-2, (d) GSTO1 (pdb 1EEM) and (e) GSTO1 with AA. (f) close-up of the AA binding site. The protein backbone is shown in cartoon form (β-strands yellow; α-helices magenta; 3_{10}-helices blue), and active-site residues in stick

form. The carbon atoms are coloured cyan (G-site residues), black (H-site residues) or orange (catalytic cysteine and ligands). Thin black lines indicate hydrogen bonds. The *cis*-peptide link between Y84 and E85 is indicated with a star (a, b).

Figure 3. Electrostatic potential surfaces of GSTO active sites. (a) structure of GSTO1 with GSH and (b) GSTO2 with GSH. The protein surfaces are colored red (negative potential) through white (neutral) and blue (positive potential).

Figure 4. Proposed mechanisms of DHAR activity. (a) DHA and the dominant hemiketal form in aqueous solution. (b) Proposed mode of binding of DHA in omega-class GSTs. (c) Proposed DHAR reaction mechanism by single electron transfer. (d) An alternative concerted mechanism for DHAR activity.

Figure 5. Structure-based sequence alignment of human GSTO2 (hGSTO2), GSTO1 (hGSTO1, PDB ID: 1EEM), fungal GSTO homolog from *Phanerochaete chrysosporium* (fGSTX, PDB ID: 3PPU) and porcine glutaredoxin (pGRX, PDB ID: 1KTE). The locations of β-strands are indicated by underlined residues, helices are indicated by strike-through. Those residues in GSTO1 interacting with AA, and their equivalents in other structures are highlighted in yellow.

Tables

Table 1. Abbreviations used for the wild-type and mutant enzymes and the mutations they contain.

Enzyme	Mutations
wtGSTO2-2	Wild-type, 243 normal residues.
GSTO2/MC6	C80S, C121S, C136S, C140S, C170S, C214S.
GSTO2/MC6D1	C80S, C121S, C136S, C140S, C170S, C214S, ΔC243 at C-terminus.
GSTO2/MC6D4	C80S, C121S, C136S, C140S, C170S, C214S, ΔFGLC at C-terminus.
GSTO2/D4	ΔFGLC at C-terminus

Table 2. Activity and kinetic analysis of various modified hGSTO2 proteins

	wtGSTO2	MC6D1	MC6D4	D4	MC6D1-E85A
Activity[a]	14.65±0.93	16.11±0.68	9.28±0.49	4.88±0.35	8.01±0.46
K_m/GSH[b]	4.82±0.83	7.80±0.46	5.97±1.32	4.18±0.93	ND
k_{cat}/GSH[c]	1.05±0.12	1.76±0.08	0.83±0.13	0.35±0.05	ND
K_m/DHA[b]	0.51±0.05	0.52±0.06	0.43±0.05	0.53±0.06	ND
k_{cat}/DHA[c]	0.66±0.03	0.81±0.04	0.48±0.02	0.28±0.01	ND

[a], nmol product/min/mg•protein; [b], mM; [c],min^{-1} ;ND, not determined.

Table 3. X-ray data collection and refinement statistics.

Structure	GSTO2/APO	GSTO2/GSH	GSTO2/GSH -2	GSTO1/AA
PDB ID	3Q18	3Q19	3QAG	3VLN
Space group	$P2_1$	$P2_1$	$P6_522$	$P3_121$
Cell dimensions				
a	46.7	46.4	53.1	56.9
b	85.7	85.0	53.1	56.9
c	60.4	60.4	352.4	140.51
	$\beta = 95.3$	$\beta = 94.6$		
Resolution range	40.85-1.70 (1.79-1.70)[c]	42.51-1.9 (2.0-1.9)	12-2.0(2.05-2.0)	30-1.70 (1.76-1.70)
Completeness (%)	93.4 (87.9)	92.9 (85.2)	98.63 (99.54)	99.2 (98.7)
Number of reflections	48429 (6623)	34258 (4571)	19842 (1428)	29768 (2912)
R_{merge}[a] (%)	4.2 (22.3)	5.4 (15.5)	8.4 (34.6)	6.1 (69.6)
I/σ	14.3 (3.5)	10.5 (3.9)	21.9 (4.6)	40.9 (4.14)
Refinement				
R-factor (%)	15.7	16.4	22.4	18.0
R_{free} (5% of data)	18.6	19.4	26.5	21.7
RMSD from ideal geometry				
Bonds (Å)	0.007	0.009	0.009	0.020
Angles (°)	1.03	1.13	1.18	1.87
Chiral volumes ($Å^3$)	0.059	0.064	0.083	0.112
Average temperature factor (B):				
Protein	11.47	22.8	22.1	17.7
Ligand		36.2	28.4	37.6
solvent	22.2	29.8	27.6	26.1
Ramachandran plot (%)[b]				
Most favoured region	98.7	97.6	97.5	98.7
Allowed region	1.1	2.2	2.1	0.9
outlier region	0.2	0.2	0.4	0.4
Residues covered by electron density:				
Protomer A	4-239	5-228	2-239	3-241
Protomer B	7-239	7-239		

[a], $R_{merge}=\Sigma\ I-\langle I\rangle\ \ \Sigma\langle I\rangle$; [b], data from Rampage [38]; [c], highest resolution bin.

Table 4. Primers used in the genetic manipulation of hGSTO2-pQE30 and hGSTO1-pHUE.

Wild type hGSTO2 primer pair [a]	Forward 5'-CAC*GGATCC*TCTGGGGATGCGACCAG-3' Reverse 5'-CTG*AAGCTT*TCAGCACAGCCCAAAGTC-3'
C80S primer pair	Forward 5'-GACCAGCCAATCTCAACTGAT-3' Reverse 5'-CATAGATCAGTTGAGATTGGCT-3'
C121S primer pair	Forward 5'-GGAGCTATTTTCTAAGGTCCCA-3' Reverse 5'-GTGGGACCTTAGAAAATAGCA-3'
C136S primer pair	Forward 5'-GGTAGCGTTGAGATCTGGGAGAGA-3' Reverse 5'-CATTCTCTCCCAGATCTCAACGCT-3'
C140S primer pair	Forward 5'-GTGGGAGAGAAAGCACTAATCT-3' Reverse 5'-CCTTCAGATTAGTGCTTTCTCT-3'
C170S primer pair	Forward 5'-CTTTGGTGGAACCTCTATATCCAT-3' Reverse 5'-CAATCATGGATATAGAGGTTCCA-3'
C214S primer pair	Forward 5'-CCCCACAGTCTCAGCTCTTCT-3' Reverse 5'-CCATGATAAGAGCTGAGACTGT-3'
C243 deleting primer	Reverse 5'-CTAATT*AAGCTT*TCACAGCCCAAAGTCA-3'
FGL deleting primer	Reverse 5'-CTAATT*AAGCTT*TCAGTCAAAGGCAT-3'
E85A primer pair	Forward 5'-GCCAATCTCAACTGATCTATGCATCTGTT-3' Reverse 5'-CACAAGCAATAACTGATGCATAGAT-3'
Y34A primer pair	Forward 5'-AGGTTCTGCCCCGCTTCTCACAGGACCCGC-3' Reverse 5'-GCGGGTCCTGTGAGAAGCGGGGCAGAACCT-3'
hGSTO1-C32S primer pair	Foreward 5'-CATGAGGTTCTCCCCGTTT-3' Reverse 5'-TCCAAGAGGGCAAACGAC-3'

[a], Note: italic *GGATCC* is a BamH1 recognition site; italic *AAGCTT* is a Hind III recognition site

Figure 1

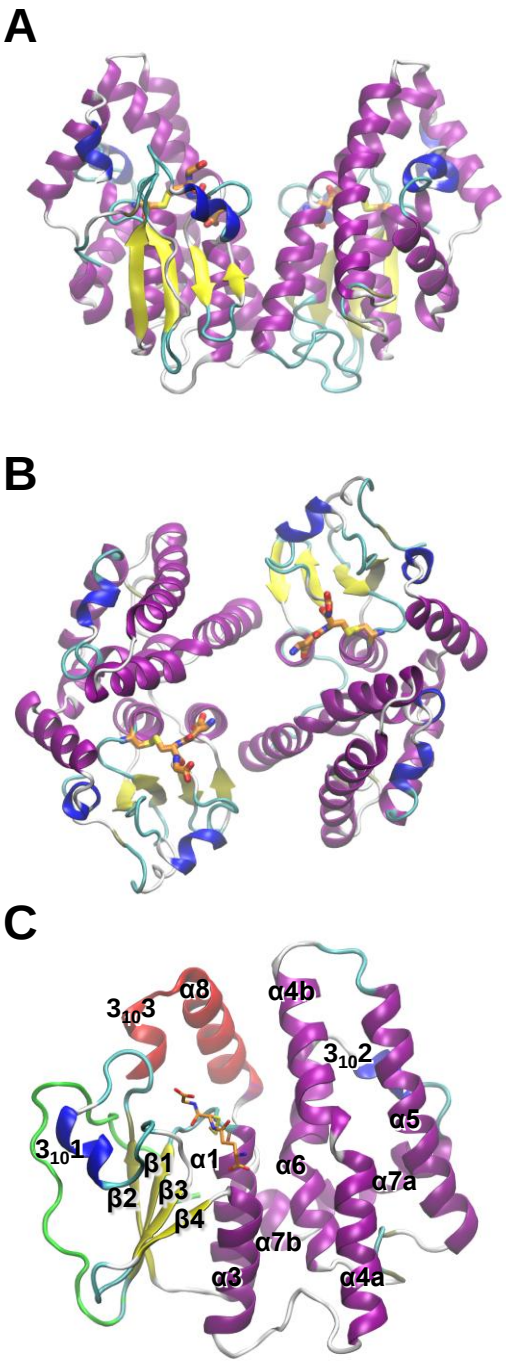

Figure 2

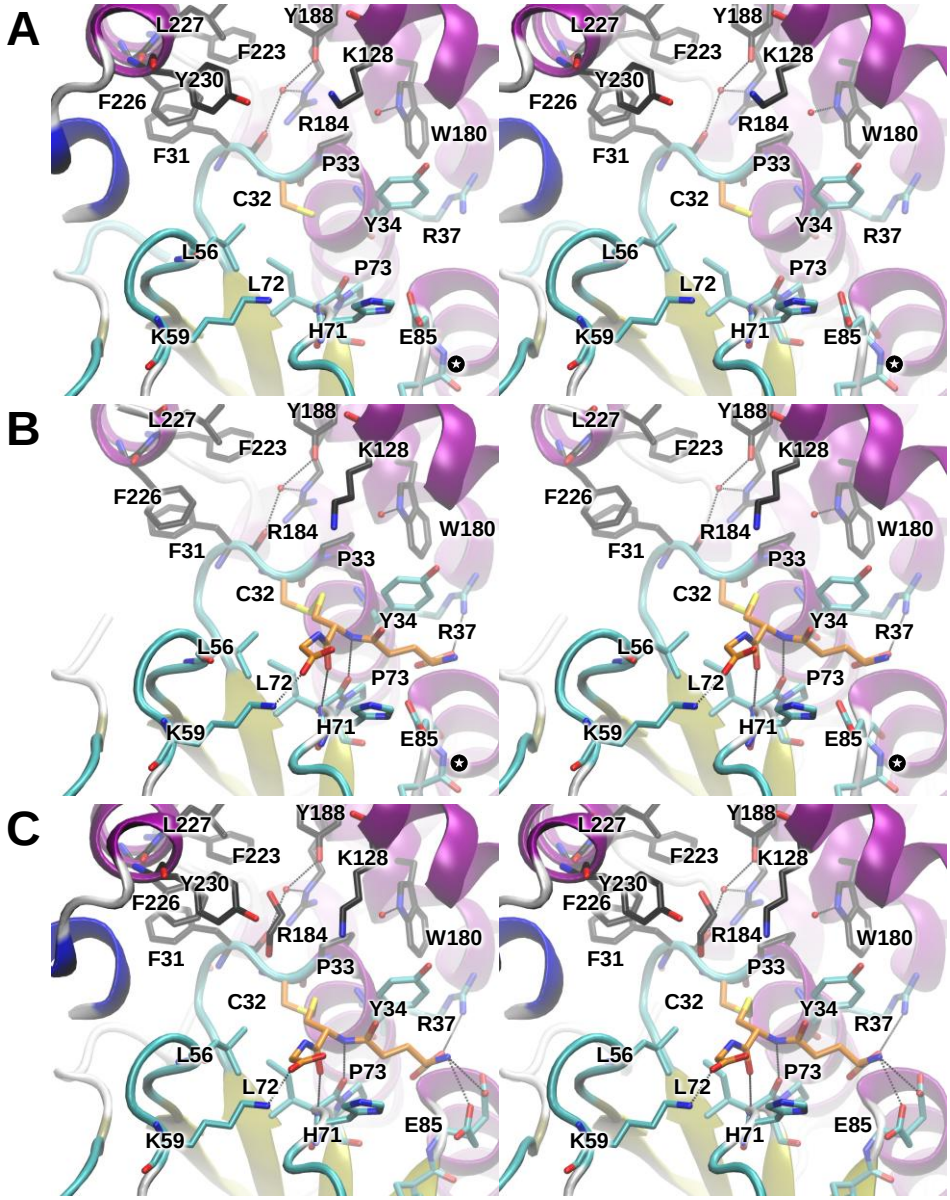
A
L227
Y188
F223
K128
Y230
F226
R184
W180
F31
P33
C32
Y34
R37
L56
P73
L72
K59
H71
E85
B
L227
Y188
F223
K128
F226
R184
W180
F31
P33
C32
Y34
R37
L56
P73
L72
K59
H71
E85
C
L227
Y188
F223
K128
Y230
F226
R184
W180
F31
P33
C32
Y34
R37
L56
P73
L72
K59
H71
E85

Figure 2DEF

Figure 2-continued

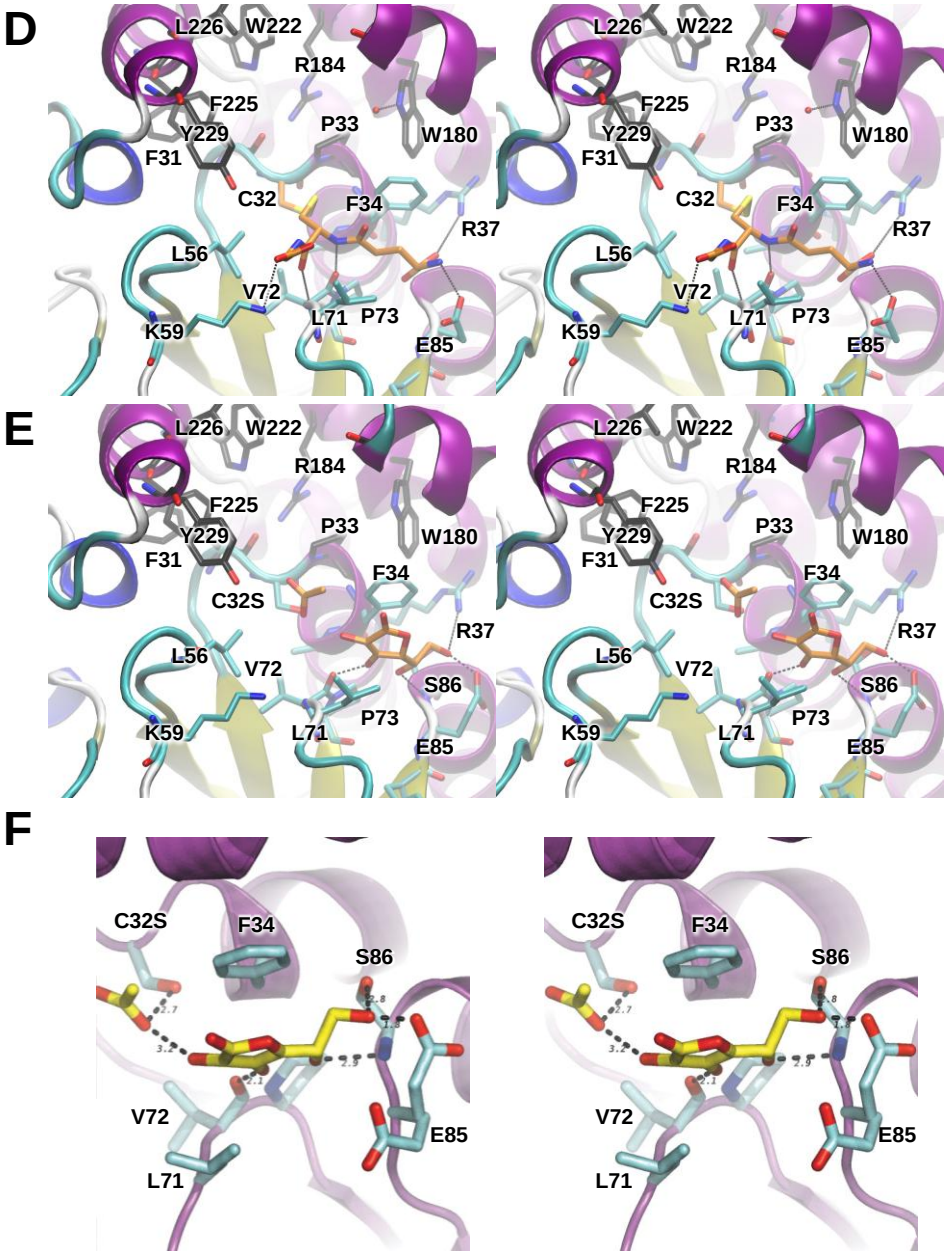

Figure 3

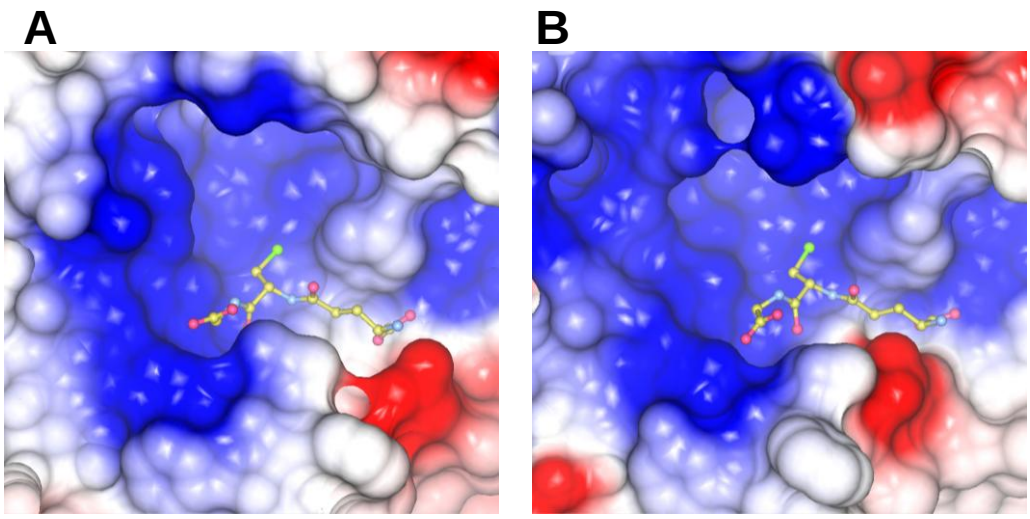

Figure 4

Figure 4

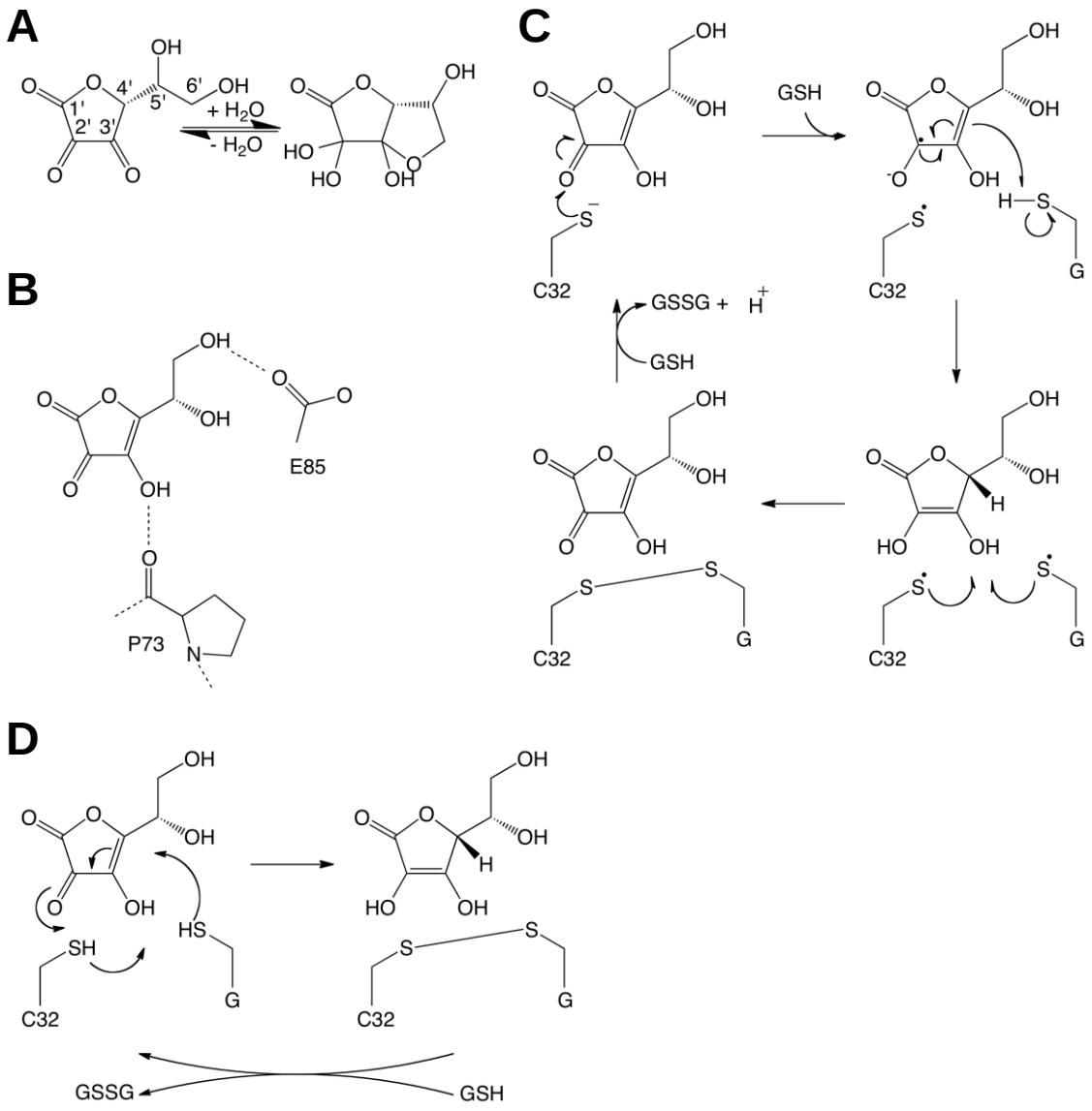

Figure 5


β1
hGSTO2 ----------msgdatrtlgkgsqppgpvpegLIRIYSMR
hGSTO1 ----------msgesarslgkgsappgpvpegSIRIYSMR
fGSTX elqsdiskmkteddgsfkrkaasfrnwiqpngdftftpekgRYHLYVSY
pGRX ----------maqafvnskiqpgKVVVFIKP
α1 β2
hGSTO2 FCPYSHRTRLVLKAKdi----RHEVvninlrnkp----------
hGSTO1 FCPFAERTRLVLKAKgi----RHEVininlknkp----------
fGSTX ACPWATRTLIVRKLKgle-dfIGVTvvsprmgsngwpfanvdpfpaads
pGRX TCPFCRKTQELLSQLpfkeglLEFVditatsdtneiqdylq--------
310 1 β3 β4 α3
hGSTO2 ----------ewyytkhpfgHIPVLEtsq--cqLIYesVIACEyl
hGSTO1 ----------ewffkknpfgLVPVLEnsq--gqLIYesAITCEyl
fGSTX dplnnaqhvkdlylkvkpdydgrfTVPVLWdkhtgtiVNNesSEIIRmf
pGRX ----------qltgarTVPRVFigk---eCIGgCTDLESmh
α4a α4b
hGSTO2 ddaypg------rklfpydpYERARQKMLLELFck-vphltkeclvalr
hGSTO1 deaypg------kkllpddpYEKACQKMILELFsk-vpslvgsfirsqn
fGSTX ntafnhllpedkakldlypeSLRAKIDEVNDWVydtvnngvyksgfast
pGRX krgelltrlqqigalk----------
α5 α6
hGSTO2 egrectnlkaaLRQEFSNLEEIleyqnttffggtcISMIDYLLWPWFER
hGSTO1 -kedyaglkeeFRKEFTKLEEVltnkkttffggnsISMIDYLIWPWFER
fGSTX -qkayeaavipLFESLDRLEKMlegq-dyli-ggqLTEADIRLFVTIVR
pGRX ----------
310 2 α7a α7b α8
hGSTO2 LDVYgildcvs-------htpALRLWISAMKw-dpTVCALlmdkSIFQG
hGSTO1 LEAMklnecvd-------htpKLKLWMAAMKe-dpTVSALltsekDWQG
fGSTX FDPVyvthfkcnlrtirdgypNLHRWMRKLYwgnpAFKDTcn-fEHIKT
pGRX ----------
310 3
hGSTO2 FLNLYfqnnpnafdfglc
hGSTO1 FLELYlqnspeacdygl
fGSTX HYFWShtfinphrivpigpipdilpld
pGRX ----------